COMPRESSIVE STABILITY STUDY OF FOUR-SIDED SIMPLY-SUPPORTED CONSTRAINED CLT WALL

Di CHEN [1], Zhao CHEN [2], Jiajia OU [3], Yi ZHANG [4], Weiguo LONG [5]

ABSTRACT: This paper aims to investigate the compressive stability performance of CLT walls. In actual engineering, CLT walls often have lateral restraints, but none of the current studies consider the effect of lateral restraints on the compressive stability performance. CLT wall was regarded as a type of orthotropic plate formed via construction, assuming a four-sided simply supported constraint, based on the orthotropic plate buckling theory , a method for calculating the buckling capability of CLT walls under uniform-compression is derived in this paper. Formulas for determining the boundary between the elasto-plastic instability and elastic instability was also proposed.The accuracy of the calculation method was verified by the CLT walls numerical models, and the overall error was found to be small. The proposed equations offer accurate predictions of the buckling capability of CLT walls under uniform-compression.

KEYWORDS: CLT, uniform compression, calculation method of buckling capability, width-to-height-ratio boundary.

1 – INTRODUCTION

This study investigates the influence of lateral constraints on the compressive stability of cross-laminated timber (CLT) walls. Within the analysis, in-plane compressed CLT structural elements are categorized into two types based on lateral constraint conditions: "one-way member" (Fig. 1 (a)) and "two-way member" (Fig. 1 (b)).

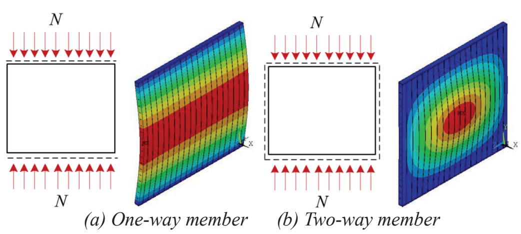

Figure 1. First-order buckling mode deformation. ('----' denotes simply supported restraint)

There many studies carried out in-depth research on the stability of CLT one-way members under axial compression. Huo [1] proposed equations for calculating the stability coefficients of CLT members under axial compression. Pina et al.[2] studied the influence of the number of laminations and openings on the buckling capability of CLT members. Perret et al. [3] deduced a normal-stress strength criterion and an additional shear strength criterion for CLT members under axial compression. Thiel et al. [4] emphasized the need to consider the bidirectional behaviors of CLT with certain boundary conditions and dimensions. Although some studies [2][3][5][6] have mentioned the concept of "walls" or "plates," lateral restraints were not considered.

As shown in the first-order modal deformation diagram of finite element analysis in Fige 1, the buckling mode of four-edge constrained CLT walls differs from that of top-bottom constrained specimens, with lateral constraints effectively restricting the wall's lateral deformation. This study therefore investigates the compressive stability of uniformly compressed CLT walls based on anisotropic plate buckling theory and establishes corresponding analytical calculation methods.

2 – CRITICAL STRESS FOR CLT WALL

This chapter solves the stable bearing capacity of the uniformly compressed CLT wall based on the theory of orthotropic plates. And it presents the method for judging its instability state. The buckling capacity refers to the

[1] Di CHEN, China Southwest Architectural Design and Research Institute Co. Ltd; ChengDu, China, sechendi@outlook.com.

[2] Zhao CHEN, China Southwest Architectural Design and Research Institute Co. Ltd; ChengDu, China, czxnsj@163.com.

[3] Jiajia OU, China Southwest Architectural Design and Research Institute Co. Ltd; ChengDu, China, ouyangjia28@126.com.

[4] Yi ZHANG, China Southwest Architectural Design and Research Institute Co. Ltd; ChengDu, China, yagiz@foxmail.com.

[5] Weiguo LONG, China Southwest Architectural Design and Research Institute Co. Ltd; ChengDu, China, xnymjg@cscec.com.

https://doi.org/10.52202/080513-0698

vertical load at which CLT walls begin to buckle. Critical stress is defined as the average stress across the wall's cross-section at this stage.

2.1 Calculation method of critical stress for CLT walls under uniform compression

The unique layered structure of cross-laminated timber (CLT) leads to markedly distinct bending stiffness in its two principal directions. When a CLT wall with four simply supported edges is subjected to uniaxial uniform compression, it demonstrates orthotropic mechanical behavior. Drawing on the buckling capacity calculation methodology for orthotropic plates, the governing differential equation for buckling can be expressed as:

$$D_1 \frac{\partial^4 \omega}{\partial x^4} + 2D_3 \frac{\partial^4 \omega}{\partial x^2 \partial y^2} + D_2 \frac{\partial^4 \omega}{\partial y^4} = N_x \frac{\partial^2 \omega}{\partial x^2} \qquad (1)$$

$$\omega = \omega_0 \sin\left(\frac{p\pi}{l_a} x\right) \sin\left(\frac{q\pi}{l_b} y\right) \qquad (2)$$

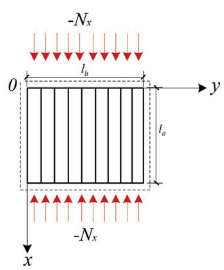

Figure 2. Diagram of CLT in-plane compression with simply supported constraints on four sides

p and q represent the number of sinusoidal half-waves in the X-direction and Y-direction, respectively, both of which are set to 1 in this study.

For CLT walls, the outer laminations are typically oriented parallel to the axial loading direction, defining the strong axis with effective flexural rigidity D_1, while the orthogonal in-plane direction constitutes the weak axis characterized by effective flexural rigidity D_2. $D_1=EI_{\mathrm{eff1}}$, $D_2=EI_{\mathrm{eff2}}$, I_{eff1} and I_{eff2} are the effective bending moments of inertia parallel and perpendicular to the loading direction, respectively.These stiffness parameters can be calculated by the γ coefficient method, with detailed calculation methods specified in Austrian and Swedish CLT design standards [6][7]. D3 is a stiffness related to torsion, it can be calculated by the semi-empirical equation $D_3 = \sqrt{D_1 D_2}$, according to the stiffness calculation method for orthotropic plates formed via construction described in Elastic Mechanics[8].

The critical stress $\sigma_{cr,e}$ for CLT walls in an elastic working state under uniform compression can be calculated by:

$$\sigma_{cr,e} = \left(\sqrt{EI_{eff1}} \left(\frac{1}{l_a}\right)^2 + \sqrt{EI_{eff2}} \left(\frac{1}{l_b}\right)^2 \right)^2 \left(\frac{\pi^2 l_a^2}{t}\right) \qquad (3)$$

Where t is the total thickness of the laminate parallel to the direction of the force.

Wood has plastic deformation capability under compression, and the CLT wall may transition into plastic states under specific loading conditions. As specified in the Chinese standard GB 50005-2017[10], the tangent modulus (E_t) should be substituted for the elastic modulus (E) when calculating critical stresses during the elastic-plastic phase analysis of structural members. This approach accounts for the variation in wood's elastic modulus E that occurs during the transition from elastic to plastic deformation behavior.

According to the GB 50005-2017, the determination of the tangent modulus (E_t) follows a standardized experimental protocol. The prescribed methodology involves performing axial compression tests on standardized specimens fabricated from designated wood species within specified quality grades, with controlled variations in slenderness ratios (λ) to establish material parameters.

The critical stress σ_{cr} is defined as the average stress at specimen failure. The tangent modulus (E_t) is subsequently derived by applying the Euler buckling formula with σ_{cr} as the input parameter. This calculation assumes a linear correlation between E_t and σ_{cr} within the elastic-plastic regime. To establish the quantitative relationship, two normalized parameters are introduced:

$$t = E_t / E \quad \text{and} \quad k = \sigma_{cr} / f$$

where E denotes the longitudinal elastic modulus and f represents the axial compressive strength of the wood. The experimentally derived *k-t* relationship, as demonstrated in Fig 3, provides fundamental data for elastoplastic analysis of timber members.

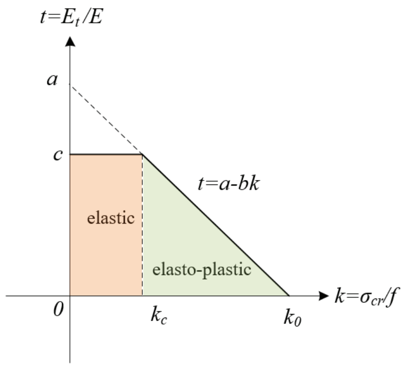

Figure 3. Relationship between parameters k and t

The k-t correlation diagram presented in Fig 3 fundamentally characterizes the intrinsic relationship between critical stress σ_{cr} and tangent modulus (Et) - essential mechanical properties inherent to the material. While CLT walls demonstrate distinct dimensional configurations and boundary constraints compared to columns, the constitutive relationship between σ_{cr} and Et remains invariant when employing identical wood species and material grading methodology. Consequently, the experimentally established k-t relationship derived from axially compressed CLT columns maintains theoretical validity for CLT wall.

The Chinese standard GB 50005-2017 provides regression-derived coefficients a_c, b_c, and c_c based on experimental data. However, the parameters a, b, c, and k_c were determined through regression analysis of the k-t relationship illustrated in Fig 3. These parameters are interrelated through the following equations:

$$a_c=c/k_0,\ c_c = \pi\sqrt{c/k_c}\ , a=bk_0, c=a-bk_c$$

By setting k_0=1.0, the full-section tangent modulus reduces to zero, resulting in instantaneous structural collapse as the critical stress reaches the material's compressive strength. Substituting the given coefficients a_c=0.91, b_c=3.13, and c_c=3.56[1], gives: a=3.13, b=3.13, c=0.91, k_c=0.709.

When CLT walls transition into the elasto-plastic regime, longitudinal laminae (parallel to the loading direction) undergo plastic deformation, while transverse laminae (perpendicular to the loading direction) retain elastic behavior. Therefore, $D_1=E_tI_{\mathrm{eff1}}$, $D_2=EI_{\mathrm{eff}}$. Substituting $E_t=(a-bk)E$, the critical stress $\sigma_{cr,p}$ governing the elasto-plastic instability of CLT walls is expressed as:

$$\sigma_{cr,p} = \left(\sqrt{(a-bk)EI_{eff1}}\left(\frac{1}{l_a}\right)^2+\sqrt{EI_{eff2}}\left(\frac{1}{l_b}\right)^2\right)^2\left(\frac{\pi^2 l_a^2}{t}\right) \quad (4)$$

Substituting $k=\sigma_{cr}/f$ into (4):

$$\sigma_{cr,p} = \left(\begin{array}{l}\left(a-b\dfrac{\sigma_{cr}}{f}\right)EI_{eff1}\left(\dfrac{1}{l_a}\right)^4\\ +2\sqrt{\left(a-b\dfrac{\sigma_{cr}}{f}\right)EI_{eff1}\left(\dfrac{1}{l_a}\right)^4 EI_{eff2}\left(\dfrac{1}{l_b}\right)^4}\\ +EI_{eff2}\left(\dfrac{1}{l_b}\right)^4\end{array}\right)\left(\frac{\pi^2 l_a^2}{t_z}\right) \quad (5)$$

Solve (5) as an equation with x as the unknown:

$$\sigma_{cr,p} = \frac{\pi^2 Ef}{\left(f+bEI_{eff1}\left(\dfrac{\pi^2}{l_a^2 t}\right)\right)^2 t} * \left(\begin{array}{l}\dfrac{2}{l_b^2}\sqrt{aI_{eff1}I_{eff2}f+bEI_{eff1}I_{eff2}\dfrac{\pi^2}{t}(aI_{eff1}\dfrac{1}{l_a^2}-I_{eff2}\dfrac{l_a^2}{l_b^4})}\\ +I_{eff2}\dfrac{l_a^2 f}{l_b^4}+aI_{eff1}\dfrac{f}{l_a^2}+bEI_{eff1}\dfrac{\pi^2}{t}\left(aI_{eff1}\dfrac{1}{l_a^4}-I_{eff2}\dfrac{1}{l_b^4}\right)\end{array}\right) \quad (6)$$

2.2 Demarcation of Elastic and Elasto-Plastic Instability Thresholds

(3) and (6) respectively present the critical stress solutions for CLT walls under uniform compression, governing elastic buckling and elasto-plastic buckling behaviors. Prior to applying these equations, a fundamental assessment of the wall's mechanical state must be conducted. In axial compression analysis, the determination of critical stress in CLT members requires initial evaluation through the limiting slenderness ratio λ_p, which serves as the bifurcation criterion between elastic and elastoplastic buckling regimes. CLT members exhibit elasto-plastic buckling behavior when the slenderness ratio λ falls below the limiting threshold λ_p, whereas elastic buckling governs structural instability at $\lambda > \lambda_p$.

The lateral restraint mechanism in CLT walls enhances material ductility by facilitating plastic deformation capacity. For members with slenderness ratios below the transition threshold ($\lambda < \lambda_p$), elastoplastic buckling invariably governs structural failure. When λ exceeds λ_p ($\lambda > \lambda_p$), the buckling mode becomes dimensionally dependent: narrow-width configurations exhibit elasto-plastic instability, while broader sections demonstrate elastic buckling characteristics. This phase transition implies the existence of a critical parameter ratio p_m demarcating elastoplastic and elastic instability domains.

It is known that elastic critical stress $\sigma_{cr,e}$ and elastoplastic critical stress $\sigma_{cr,p}$ should be equal at this

https://doi.org/10.52202/080513-0698

transitional boundary. By establishing the parametric relationship $I_{eff2}\left(\frac{1}{l_b}\right)^4 = nI_{eff1}\left(\frac{1}{l_a}\right)^4$ (where n represents the dimensionless proportionality factor), the equality condition $\sigma_{cr,e}$ = $\sigma_{cr,p}$ yields an equation system for determining the critical transition ratio p_m. Solving yields the following equation:

$$EI_{eff1} = \frac{f(a-1)l_a^4 t}{\pi^2 b l_a^2\left(1+n+2\sqrt{n}\right)} \quad (7)$$

Substituting $I_{eff2} = mI_{eff1}$ into (7):

$$EI_{eff1}\left(\frac{1}{l_a}\right)^2 \frac{\pi^2}{t}\frac{b}{f}\left(1+m\left(\frac{l_a}{l_b}\right)^4+2\sqrt{m}\left(\frac{l_a}{l_b}\right)^2\right)=(a-1) \quad (8)$$

Solve (8) as an equation with p_m ($p_m = l_b / l_a$)as the unknown:

$$p_m = \sqrt{\frac{b\pi EI_{eff2}}{\left(l_a\sqrt{ftb(a-1)EI_{eff2}} - b\pi E\sqrt{I_{eff1}I_{eff2}}\right)}} \quad (9)$$

The instability classification of CLT walls follows dual criteria:

(a) for $\lambda \leqslant \lambda_p$, elastoplastic buckling governs regardless of width of the CLT wall.

(b) When $\lambda > \lambda_p$, the transitional aspect ratio p_m obtained from Eq. (9) determines failure modes:

- R$\leqslant p_m$, Elastoplastic instability dominates.
- R> p_m, Elastic instability prevails.

where R denotes the width-to-height-ratio of CLT wall.

3 –FINITE ELEMENT ANALYSIS AND RESULTS

In previous axial compression tests of CLT members[1], the specimens were fabricated using visually graded hemlock dimension lumber with No.1-grade laminations. The nominal cross-section dimensions were 2"×6" (38 mm × 140 mm), planed to an actual thickness of 35 mm per layer, and the total thickness of the CLT member was 105 mm.

The finite element analysis of CLT walls in this study adopted the same material parameters and lamination layup configurations as those used in the axial compression tests[1]. Prior to this study, the finite element model was validated against experimental tests. The established finite element model demonstrates good capability in accurately simulating the mechanical behavior of CLT components.

Hemlock's elastic constants were established through CSA O86-19 [11] and Mechanical Properties of Wood [12], $E_{//}$ =11000Mpa, $G_{//}$ =687.5Mpa, v_{12}=0.423, v_{13}=0.485, v_{23}=0.382(v is the Poisson's ratio). The orthotropic material relationships follow:

- Transverse elastic modulus: $E_{\perp}=E_{//}/30$.
- Shear modulus: $G_{//}=E_{//}/16$.
- Rolling shear modulus: $G_{rt}=G_{//}/10$.

The strength data of the hemlock dimension lumber were sourced from Canadian Lumber Properties [14] and NDS - 2018[15]. The rolling shear strength is set as one - third of the shear strength parallel to the grain. Additionally, the tensile strength perpendicular to the grain is 1/3 of the shear strength perpendicular to the grain. The average strength values are presented in Table 1.

Table 1 Average values of strengths of hemlock dimension lumber

	Parallel to grain	Perpendicular to grain
Tensile strength (MPa)	24.20	1.03
Compressive strength (MPa)	35.20	4.60
Shear strength (MPa)	3.10	1.03

The parametric modeling was performed using the 8-node SOLID185 element in ANSYS software, accounting for the orthotropic characteristics of wood. A 4mm interlayer gap was defined between CLT laminae, with each lamina divided into four mesh layers. The finite element model of the CLT wall is shown in Figure 4, subjected to simply supported boundary conditions on all four edges.

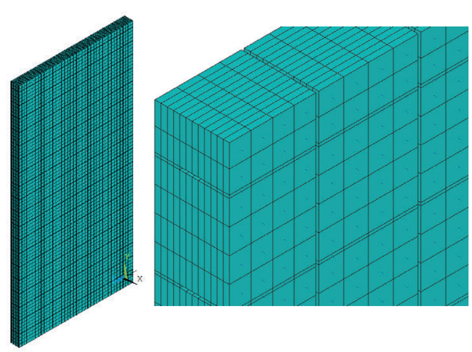

Figure 4. CLT wall finite element model

In the present study, the numerical model of CLT is formulated with the utilization of an ideal elastoplastic constitutive model and the Hill yield criterion. The stress - strain relationship of wood in the direction parallel to the grain, which is illustrated in Fig. 6, is described by means of the Multilinear Isotropic Hardening (MISO) model implemented within the ANSYS software environment. Considering the evolution of plasticity under longitudinal compression, the ultimate compressive strain is defined as ε_u = - 0.008.

An eigenvalue buckling analysis was first conducted, incorporating the first-order buckling mode deformation of the CLT wall scaled to L/1000 as the initial geometric imperfection(L is the height of the CLT wall). Subsequently, displacement-controlled loading was applied until structural failure occurred. The peak load value on the load-displacement curve was identified as the critical buckling load.

Finite element models of CLT walls with different aspect ratios were established, comprising three laminations with each layer thickness of 35 mm. The walls maintained a constant height of 2800 mm while varying in width from 1400 mm to 14000 mm. These models were categorized into six groups designated as W1-W6. Two types of boundary conditions were investigated: fully simply-supported (all four edges) and partially constrained (only top and bottom edges simply-supported), with comparative analysis performed on critical stresses under both constraint scenarios. The vertical load values from each set of finite element analysis results were normalized to unit width. The normalized load-displacement curves were plotted in the same figure, as shown in Fig 5.

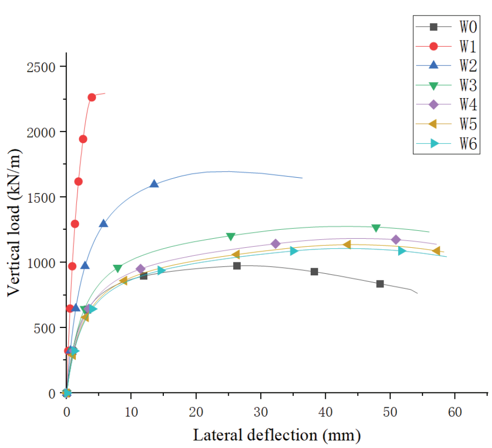

Figure 5. Load-displacement curve of CLT wall finite element analysis

Note: W0 was constrained only at the top and bottom edges, while models W1 to W6 were fully constrained on all four edges.

Fig 1 illustrates the first-order buckling mode deformations of CLT walls under uniform compression with different boundary conditions. The buckling deformation patterns for CLT walls with varying width-to-heigh ratios remain analogous to those shown in Fig 1. Theoretical critical stress values for each CLT wall were calculated using Equation (3) or (6). Table 2 presents the critical stresses obtained from numerical simulations and theoretical calculations respectively, with relative errors determined by taking finite element method (FEM) simulation results as the benchmark.

Table 2 Finite element analysis and theoretical calculation results of CLT walls with different width-to-height ratios

	Width	$\sigma_{cr,co}$ (MPa)	$\sigma_{cr,fe}$ (MPa)	Increase (%)	$\sigma_{cr,th}$ (MPa)	Relative error (%)
W1	1400	14.83	32.78	121.05%	31.75	-3.13
W2	2800	14.83	24.24	63.47%	24.12	-0.47
W3	5600	14.83	18.23	22.94%	18.59	2.01
W4	8400	14.83	16.91	14.07%	17.60	4.06
W5	11200	14.83	16.24	9.49%	17.26	6.31
W6	14000	14.83	15.82	6.71%	17.10	8.10

Note: $\sigma_{cr,co}$ is the FEA critical stress under top-bottom edge constraints only; $\sigma_{cr,fe}$ is FEA critical stress under four-edge constraints; $\sigma_{cr,th}$ is the theoretical critical stress under four-edge constraints.

The dimensions of CLT walls in groups W2 and W3 approximate those commonly used in engineering practice. When subjected to four-edge constraints, these walls exhibit significantly enhanced load-bearing capacity. Adopting the calculation methodology proposed in this study for engineering design could effectively optimize material utilization, which holds substantial significance for cost reduction in construction projects.

When the CLT wall was constrained with simply supported conditions at the top and bottom edges only, it exhibited unidirectional structural behavior. The unit-width normalized vertical load remained invariant to aspect ratio variations, with deviations among the W1-W6 groups all within 1%. Numerical simulations reveal that lateral restraints enhance the critical stresses of CLT walls, with a diminishing enhancement effect observed as the width-to-height ratio increases. Calculated from (9), the width-to-height ratio threshold (p_m) was 1.02. Specimen groups W1 and W2 exhibited elasto-plastic instability behavior, while groups W3-W6 demonstrated elastic instability characteristics, Which is consistent with the results of the finite element analysis.

With increasing width-to-height ratios, the constraining efficacy of lateral restraints on mid-wall regions progressively diminishes. This restraint reduction induces two concurrent mechanisms: (1) potential tensile failure initiation in central timber laminations, and (2) gradual contraction of the effective compression zone. These synergistic effects amplify lateral deformations beyond theoretical predictions, while simultaneously reducing the mid-wall bearing capacity below calculated values. Consequently, the discrepancy between theoretical and numerical results escalates proportionally with width-to-

https://doi.org/10.52202/080513-0698

height ratios. Maximum relative error in theoretical critical stress predictions reached 11.92%, though overall deviations remained within acceptable limits, demonstrating strong congruence between analytical solutions and finite element method (FEM) simulations.

The overall error of Numerical Models were small, indicating that the proposed calculation method is applicable to calculate the critical stresses of multilayer CLT walls under uniform compression.

4 – CONCLUSIONS

Unlike methods calculating the buckling capacity of CLT walls based on unidirectional component theory, this study investigates the influence of lateral constraints on CLT wall buckling capacity using plate buckling theory. Based on the buckling theory of orthotropic thin plates, we derive a calculation formula for the buckling capacity of CLT walls under uniform compression.

Finite element analysis reveals that lateral constraints can significantly enhance the buckling resistance of CLT walls. Neglecting lateral constraints in engineering design may lead to substantial material waste. The buckling patterns suggest that plate component theory should be adopted for studying the buckling capacity of laterally constrained CLT walls. Future research should further explore the effects of different constraint conditions on the compressive stability of CLT walls.

The theoretical calculations demonstrate small overall error compared with numerical simulations, indicating that the derived equations can effectively predict the buckling capacity of uniformly compressed CLT walls.

This paper categorizes uniformly compressed CLT walls into elastic and elastoplastic buckling modes. A stability boundary determination method is proposed, considering the effects of slenderness ratio and width-to-height ratio on load-bearing capacity. The developed equations provide a novel conceptual framework and methodology for calculating CLT wall buckling capacity under uniform compression, facilitating the broader application of CLT in multi-story timber structures.

5 – REFERENCES

[1] Huo LL, Wu GF, Wang HJ, Zhu EC. Calculation of the stability coefficient of Cross-Laminated Timber members in axial compression. J Build Struct 2021; 42(08):107-116. https://doi.org/10.14006/j.jzjgxb.2019.0818.

[2] Pina JC, Flores EIS, Saavedra K. Numerical study on the elastic buckling of cross-laminated timber walls subject to compression. Constr Build Mater 2019; 199:82-91. https://doi.org/10.1016/j.conbuildmat.2018.12.013.

[3] Perret O, Douthe C, Lebee A, Sab K. A shear strength criterion for the buckling analysis of CLT walls. Eng Struct 2020; 211. https://doi.org/10.1016/j.engstruct.2020.110344.

[4] Thiel A, Krenn H. Buckling loads for cross-laminated timber elements under uniaxial in-plane compression. In: Proceedings of the World Conference on Timber Engineering (WCTE2016), Vienna, Austria; 2016.

[5] Huang ZR, Huang DS, Chui YH, Shen YR, Daneshvar H, Sheng BL, Chen ZF. Modeling of Cross-Laminated Timber (CLT) panels loaded with combined out-of-plane bending and compression. Eng Struct 2022; 250. https://doi.org/10.1016/j.engstruct.2021.113335.

[6] Heinisuo M, Pajunen S, Aspila A. Ultimate failure load analysis of cross-laminated timber panels subjected to in-plane compression. Struct 2022; 47:1558-1565. https://doi.org/10.1016/j.istruc.2022.12.016.

[7] proHolz Austria. Cross-Laminated Timber Structure Design. Immenstadt, Germany: Eberl Print; 2014.

[8] Swedish Wood. The CLT Handbook—CLT structures—facts and planning. Skelleftea: Föreningen Sveriges Skogsindustrier; 2017.

[9] Xue ZL. Elastic Mechanics. Fourth edition. Beijing, China: Higher Education Press; 2006.

[10] GB 50005—2017. Standard for design of wood structures. Beijing, China: China Architecture and Building Press; 2017.

[11] CSA O86—19. Engineering design in wood. Association: Toronto Canadian Standards; 2019.

[12] Green DW, Winandy JE, Kretschmann DE. Chapter 04: Mechanical Properties of Wood. Wood Handbook—Wood as an engineering material. Madison, Wisconsin: Forest Products Laboratory; 1999.

[13] Pan JL, Zhu EC. Principles of wood structure design. Second edition. Beijing, China: China Architecture and Building Press; 2019.

[14] Barrett JD, Lau W. Canadian Lumber Properties. Canada: Canadian Wood Council; 1994.

[15] NDS—2018. National Design Specification (NDS) for Wood Construction 2018 Edition. Washington DC: American Forest & Paper Association, American Wood Council; 2018.